JOURNAL OF SPACECRAFT AND ROCKETS
Vol. 38, No. 2, March–April 2001

Experimental Analysis of Aerodynamic Interactions Occurring on Hypersonic Spacecraft

Philippe Reijasse,* Reynald Bur,† and Bruno Chanetz†
ONERA, F-92320 Châtillon, France

Experimental investigations have been achieved in the ONERA research facilities of the Chalais–Meudon Center in order to validate design tools used for the definition of a scramjet for a hypersonic spacecraft. Aerodynamic interactions occurring on such a spacecraft have been thoroughly studied, notably 1) the shock/shock interactions ahead of the air inlets, 2) the shock-wave/boundary-layer interaction and its control inside the air inlet, and 3) the flow confluence between an external flow and an aerospike nozzle jet in an underexpansion condition. These studies contribute to the knowledge of the flow physics of aerodynamic interactions that occur on hypersonic spacecraft, compensate for the lack of published detailed measurements of such flowfield patterns, and provide well-documented test cases to validate computer codes.

Nomenclature

p_B	=	base pressure, Pa
p_e	=	external flow static pressure, Pa
p_j	=	jet static pressure, Pa
p_{te}	=	external flow stagnation pressure, Pa
p_{tj}	=	jet stagnation pressure, Pa
$p_{t\,ref}$	=	stagnation pressure in the reference case, Pa
p_w	=	wall pressure, Pa
Q	=	suction mass flow rate, kg/s
T_{te}	=	external stagnation temperature, K
u_e	=	upstream reference velocity, m/s
u, w	=	instantaneous streamwise and normal/radial velocity components, m/s
u', w'	=	fluctuating streamwise and normal/radial velocity components, m/s
θ	=	angle relative to the horizontal plane, deg
ρ	=	specific mass, kg/m^3
σ_u	=	streamwise turbulence intensity, $\sigma_u = \sqrt{(\overline{u'^2})}/u_e$
Φ	=	heat-flux, W/m^2

Introduction

HYPERSONIC airbreathing spacecraft will be one of the largest technological challenges in the aeronautical community during the twenty-first century. The key to this type of transportation is the technological mastery of the propulsion system. The thin, pointed bodies of hypersonic spaceplanes, as shown in Fig. 1a, are designed to minimize drag and to optimize engine efficiency. The taper of the forward part of the body plays the role of a compression ramp that reduces the flow speed ahead of the air inlet to increase propulsion efficiency. The contour of the afterbody is designed as an expansion surface and acts as a propulsive nozzle. In the framework of the French Program of Research for Advanced Hypersonic Propulsion (PREPHA), experiments were conducted at the ONERA research facilities to validate the design tools used to derive these vehicle configurations.

The conception of the air inlet must take into account two major aerodynamic interactions. First, certain shock/shock interaction phenomena ahead of the air inlet lip (Fig. 1b) generate high local heat fluxes, which fluxes can be limited by the blunt shape of the lip. These shock/shock interactions, which result from the intersection of shocks produced by the compression ramp with the bow shock forming ahead of the lip, are classified as six types according to Edney.[1,2]

1) Types I and II: When the oblique shock crosses the bow shock, in the area where it is a strong shock, the two shocks have very different strengths, and a slip line results from this interaction.

2) Type III: When reattachment of the slip line is possible on a surface, the situation is categorized as a type III interaction.

3) Type IV: When reattachment is not feasible, the slip line is followed by a supersonic jet surrounded by a subsonic flow. When the supersonic jet impacts a cylinder, the situation corresponds to type IV interaction (as shown in the Electron Beam Fluorescence visualization in Fig. 2 and explanation in Ref. 3).

The purpose of this paper is to present the results of an experimental analysis of type III and type IV interactions, which induce the most significant consequences in terms of wall pressure and heat-flux increases.

Second, the strong interactions occurring inside the air inlet between oblique shock waves and turbulent boundary layers (Fig. 1b) induce a loss of propulsion efficiency. One way to reduce the adverse effects of such interactions is to use a control device near the impingement region of the shock on the air inlet wall. A review of several control devices[4,5] indicates that active control by suction of the inner part of the boundary layer is an efficient control technique for such interactions. The objective of this experimental study was to contribute to the understanding of the physical phenomena involved in shock-wave/boundary-layer interactions under active control (suction) conditions. Two means of suction control have been explored in this study: distributed suction through a perforated plate and localized suction through a slot.

The shape of the expansion surface constituting the aft part of the vehicle must take into account the complex interactions due to flow confluence between the propulsive jet and the outer flow (Fig. 1b). In general, the coflowing streams are nonadapted, which, in supersonic or hypersonic regimes, generates shock waves interacting with the dissipative layers. When the flows are far from the adaptation state, the strength of the interaction shock can be so severe that it forces the external flow to separate because of the jet's expansion (pluming). Another aerodynamic interaction can occur when the confluence process forces the jet internal shock to impinge on the expansion surface. These nonadaptation phenomena induced by flow confluence have an influence on the afterbody drag and thrust balance, on the aerodynamic stability and maneuverability of the vehicle when unstable flow separation is induced by the jet pluming, and on the base heat-flux levels because hot gases are present inside the separated fluid regions. The aim of the present experimental study is to increase the understanding of the flow physics of the confluence between an external stream and a propulsive jet exhausting from an expansion surface. An annular expansion nozzle, rather

Presented as Paper 99-0610 at the 37th Aerospace Sciences Meeting, Reno, NV, 11–14 January 1999; received 22 June 1999; revision received 14 March 2000; accepted for publication 18 March 2000.

*Research Scientist, Fundamental/Experimental Aerodynamics Department, 8 rue des Vertugadins, Meudon. Member AIAA.

†Research Scientist, Fundamental/Experimental Aerodynamics Department, 8 rue des Vertugadins, Meudon.

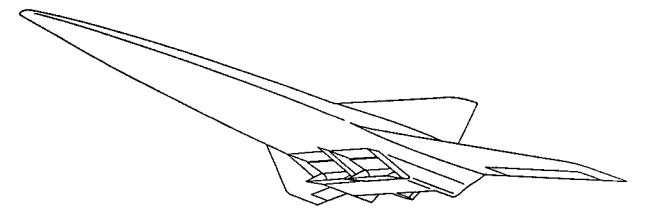

a) Typical hypersonic spacecraft

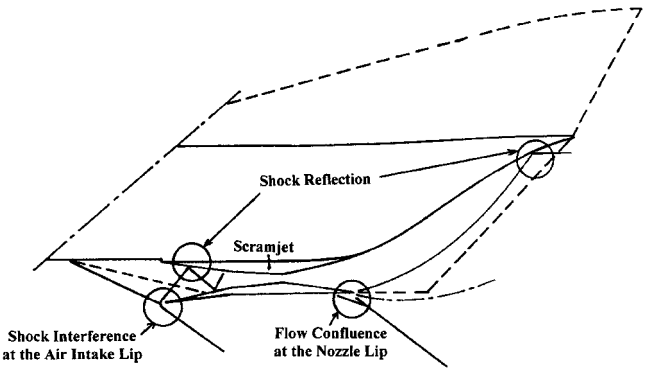

b) Aerodynamic interactions

Fig. 1 Basic aerodynamic phenomena studied.

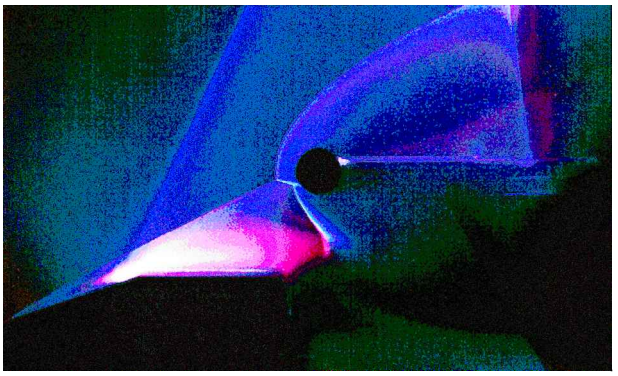

Fig. 2 Visualization of the type IV interaction by electron beam fluorescence.

than a planar one, was chosen to facilitate the validation procedure with numerical codes; therefore, the experiments were conducted using an axisymmetric afterbody model equipped with a full-length annular aerospike nozzle and merged in a supersonic external flow.[6]

Shock/Shock Interactions Ahead of the Air Inlet Lip

Experimental Arrangement

The experimental study was performed in the ONERA R5Ch blowdown wind tunnel.[7] The facility provides a uniform flow at Mach 10, where stagnation temperature and pressure are 1070 ± 10 K and $(2.5 \pm 0.15) \times 10^5$ Pa, respectively. The freestream static conditions are $p_e = 6.3$ Pa, $T_e = 52$ K, and $\rho_e = 4.3 \times 10^{-4}$ kg/m^3. Because of the low stagnation pressure, the unit Reynolds number is $Re_u = 1.67 \times 10^5$, resulting in a fully laminar flow.

The experimental arrangement includes a shock generator with a sharp leading edge located in front of a cylinder lying perpendicular to the upstream flowfield (Fig. 2). The shock generator is a 10-deg wedge with a 100-mm base. For the present experiment, the wedge is at 10 ± 0.01 deg incidence angle, which induces a 20-deg flowstream deflection angle.[8] The cylinder has a diameter of 16 mm and a spanwise length of 100 mm. The ratio of spanwise length to diameter is greater than six, which ratio is sufficient to insure a two-dimensional flow near the middle of the cylinder in the region where the thermocouples and pressure taps are located.

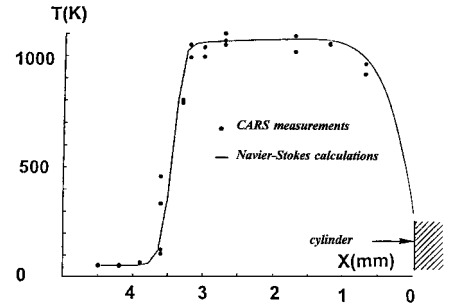

Fig. 3 Axial distribution of temperature on the stagnation line: reference case.

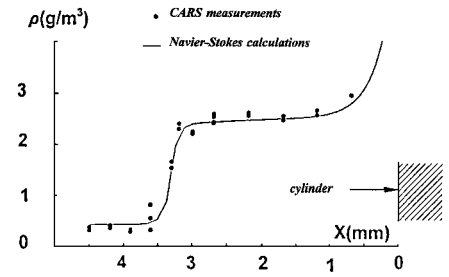

Fig. 4 Axial distribution of density on the stagnation line: reference case.

Results

First, the reference case is discussed. The cylinder alone in the flow producing a bow shock was considered. The detached shock area in front of the cylinder was probed using dual-lines anti-Stokes–Raman scattering (DLCARS).[9] Figure 3 shows the axial distribution of rotational temperature along the stagnation line. Because rotational equilibrium is reached after a few collisions between molecules for the R5Ch wind tunnel conditions, the rotational temperature is assumed to be equivalent to the static temperature. The temperature jump due to the shock, particularly intense at large Mach number, is in good agreement with the numerical results obtained with Navier–Stokes calculations (ONERA-Homard2 solver; Ref. 10). This code numerically solved the dimensionless unsteady Navier–Stokes equations written in Cartesian coordinates. The system of Navier–Stokes equations is discretized in a curvilinear mesh by an implicit finite volume method. The inviscid fluid terms, including a "flux limiter"-type correction, are treated by the Harten–Yee method based on the total variation diminishing scheme for solving the Euler equations. The viscous fluid-flux terms are taken into account by a space-centered scheme similar to the Crank–Nicolson scheme in which the space derivative of the velocity and energy are calculated in the middle of each cell with a formula including six points. This code has been validated on two-dimensional ramp configurations[7] and also tested in the R5Ch wind tunnel under the same flowstream conditions as those encountered in this study.

Specific mass, deduced from the CARS probing along the stagnation line, is presented in Fig. 4. The good agreement between calculation and experiment illustrates the validation of the measurement technique and the accuracy of the continuum approach used to solve the conservation equation for mass, momentum, and energy (Navier–Stokes equations). The accuracy of the measurements made using CARS depends on the probing location considered. In points of the flow that are not disturbed by heating of the model, the measurement accuracy was equal to 2%, but for points located near the wall, the measurement accuracy was around 15%.

Subsequently, the type III and type IV interaction cases were tested by adding a shock generator in front of the cylinder to produce a shock impinging on the bow shock. The most spectacular effect resulting from shock/shock interactions was the occurrence of pressure and heat-flux peaks at the wall due to the effect of the impinging shear layer (type III) or of the supersonic jet (type IV). (As Edney[1] observed, "Anomalous heat transfer and pressure

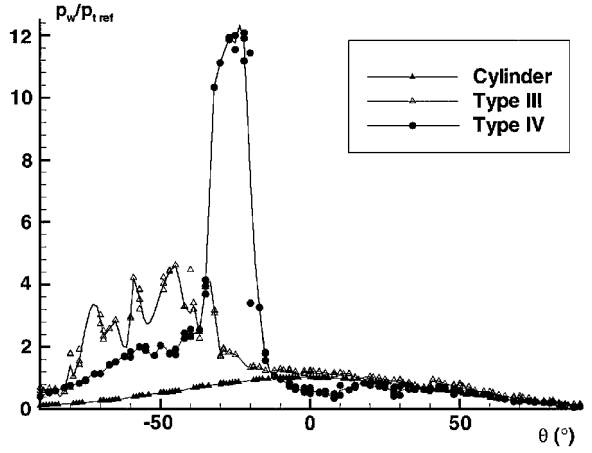

Fig. 5 Pressure distribution around the cylinder.

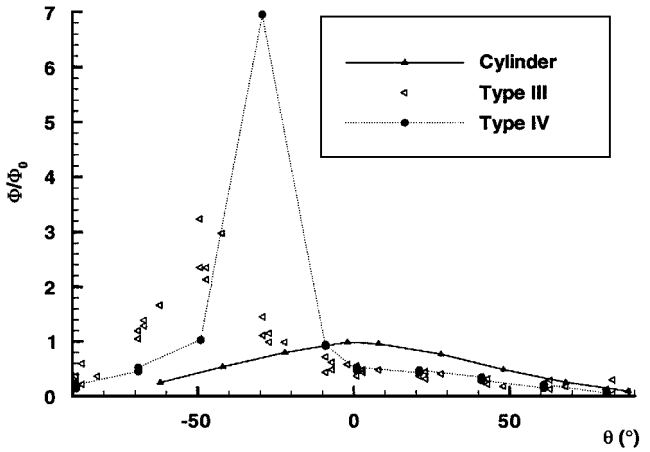

Fig. 6 Heat-flux distribution around the cylinder.

distributions on blunt bodies at hypersonic speeds in the presence of an impinging shock.") This problem has also recently been studied in detail by a large number of scientists (for example, in Ref. 11). Figure 5 presents the circumferential distribution of wall pressure on the cylinder for the reference case and the two interaction types studied. Wall pressures p_w were nondimensionalized by the stagnation pressure $p_{t\,\mathrm{ref}}$ measured at the stagnation point in the reference case. The accuracy of the pressure measurements is $\pm 5\%$. The curve relative to type III interaction exhibits a pressure peak $p_w/p_{t\,\mathrm{ref}} = 2.6$ at $\theta = -45$ deg, and the curve relative to type IV interaction exhibits a pressure peak $p_w/p_{t\,\mathrm{ref}} = 7.6$ at $\theta = -25$ deg. Figure 6 shows the circumferential heat-flux distribution around the cylinder. The results are divided by $\Phi_{\mathrm{ref}} = 65{,}000\ \mathrm{W/m^2}$, the experimental value obtained at the stagnation point on the cylinder in the reference case without the impinging shock. The accuracy of heat-flux measurements is $\pm 7\%$. The heat-flux peak observed for the type III pattern is three times higher than the heat-flux measured at the stagnation point in the reference case, whereas the heat-flux peak for the type IV pattern reaches seven times the reference value. These values are indicative of the significance of the problems encountered in this region. In addition to wall measurements, the DLCARS technique has also been used to analyze the flow. Rotational temperature and nitrogen number density were measured along 9 lines in front of the cylinder, constituting a total of 125 points. These results have been compared in Ref. 12 with calculations using direct simulation Monte Carlo (DSMC) code.

Shock-Wave/Boundary-Layer Interaction and Control Inside the Air Inlet

Test Setup and Equipment

These experiments were conducted in the ONERA S8Ch research wind tunnel.[13] This facility is a continuous wind tunnel supplied with desiccated atmospheric air. The nozzle provides a nominal Mach number of 1.95, and the test section has dimensions of 120×120 mm. A shock generator with a sharp leading edge is fixed at the upper wall of the wind tunnel nozzle and creates an oblique shock wave that impinges on the lower wall. A 7-deg shock generator angle of incidence was selected to test the control devices. The resulting oblique shock wave had a moderate intensity, which generates an interaction region with an incipient separation of the boundary layer. The lower wall was equipped with the active control device, which included 1) a cavity closed by a 100-mm-length perforated plate, connected to a vacuum pump for distributed suction control, or 2) a 5-mm-length slot located in the shock impingement region to provide a localized suction control.

The suction mass flow rates were measured by the use of sonic throats, the mass flow rate Q being fixed by the diameter of the sonic throat. Two values of Q have been tested, corresponding respectively to 1) a moderate suction ($Q = 0.016$ kg/s), which corresponds to around 0.8% of the incoming wind tunnel mass flow rate, and 2) a strong suction ($Q = 0.031$ kg/s), which is equivalent to 1.5% of the wind tunnel mass flow rate.

The flows were analyzed using schlieren visualizations, measurements of wall pressure distributions, and instantaneous velocity probings obtained with a two-component laser Doppler velocimetry (LDV) system.[14] The flow was seeded with micron-sized particles of magnesium monoxide (MgO) injected in the wind-tunnel settling chamber. Reliable measurements with this LDV system were limited to a minimum distance of 0.3 mm from the wall. The flowfield properties were determined with a precision of 1% of the maximum velocity modulus for the mean velocity components and less than or equal to 10% for the components of the Reynolds tensor.

Results

A schlieren visualization of the interaction region for the reference case without control is shown in Fig. 7. This photograph reveals the characteristic features of a shock-wave/boundary-layer interaction of moderate intensity, i.e., without (or with incipient) boundary-layer separation.[15] The incident shock-wave curves inward as it passes through the supersonic part of the boundary layer. At the same time, the interaction process upstream causes the subsonic part of the boundary layer to thicken, which thickening creates compression waves that focus and form the reflected shock wave. The penetration of the incident shock wave into the boundary layer leads by refraction to the formation of a broad expansion fan just downstream of the reflected shock wave.

Additional results, including mean flowfield properties, were deduced from the LDV measurements. Figure 8 shows contour lines of Mach number for the reference case without control. This illustrates the structure of the wave system previously shown in the schlieren photograph, but attention is drawn to the structure of the viscous part of the flow. The phenomenon entails a rapid expansion of the subsonic portion of the boundary layer. The sonic line, very close

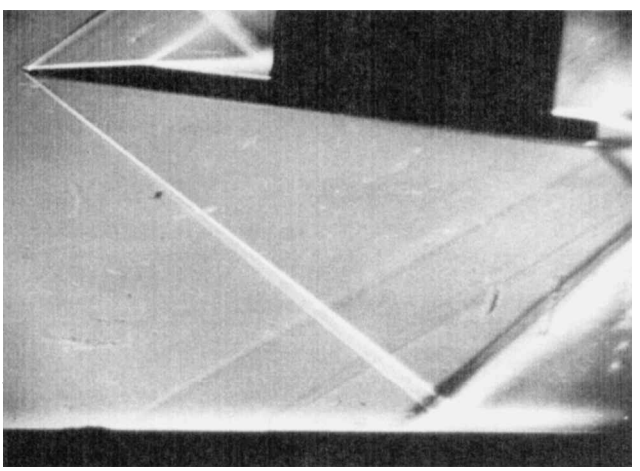

Fig. 7 Schlieren photograph of the interaction region: reference case (without control).

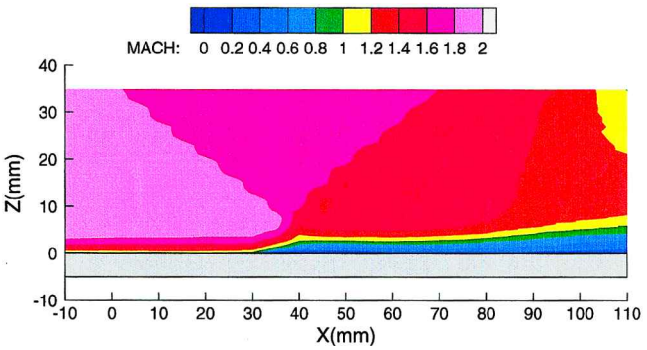

Fig. 8 Mach number contour lines: reference case (without control).

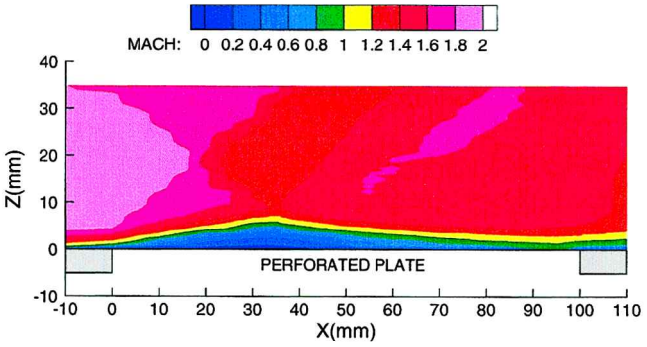

a) Control case by suction through a perforated plate (Q = 0.016 kg/s)

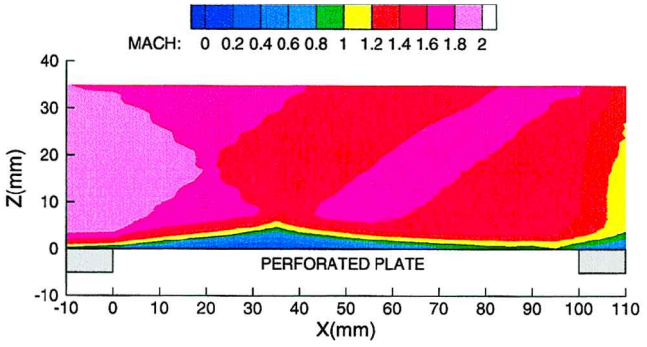

b) Control case by suction through a perforated plate (Q = 0.031 kg/s)

Fig. 9 Mach number contour lines.

to the wall at first, rises up into the dissipative layer downstream of the interaction region. Figure 9 shows the Mach contour lines for the distributed suction control case with moderate mass flow rate ($Q = 0.016$ kg/s) and strong mass flow rate ($Q = 0.031$ kg/s). These plots reveal a significant change in the structure of the wave system, the latter being similar to a strong shock-wave/boundary-layer interaction under passive control (i.e., natural circulation under the perforated plate), well defined in the transonic regime.[16,17] The rapid thickening of the boundary layer, which is induced by the injection effect taking place in the upstream part of the control region, is felt by the contiguous supersonic flow as a ramp effect. This effect then leads to the formation of the reflected shock wave, whose location at the perforated plate origin is far upstream from that of the reference case. Thus, the smearing of the shock system and splitting of the compression achieved by the interaction have the beneficial effect of reducing the efficiency loss of the air inlet. However, the thickening of the boundary layer leads to an increase in the momentum loss. This negative effect is slightly limited by the natural suction operated in the downstream part of the perforated plate. It is evident that the boundary layer at the aft portion of the perforated plate has recovered the incoming boundary-layer characteristics when the strong mass flow rate is applied (Fig. 9b). Figure 10 shows the Mach contour lines for the localized suction (by

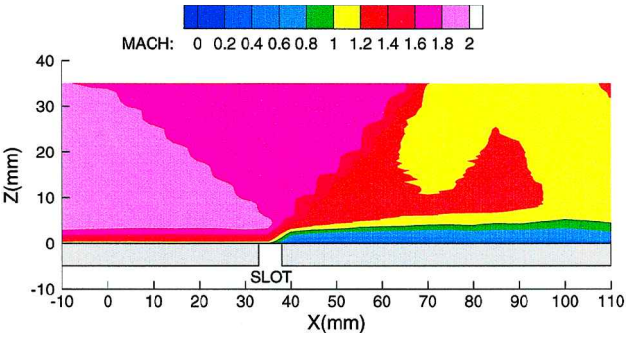

Fig. 10 Mach number contour lines: control case by slot suction.

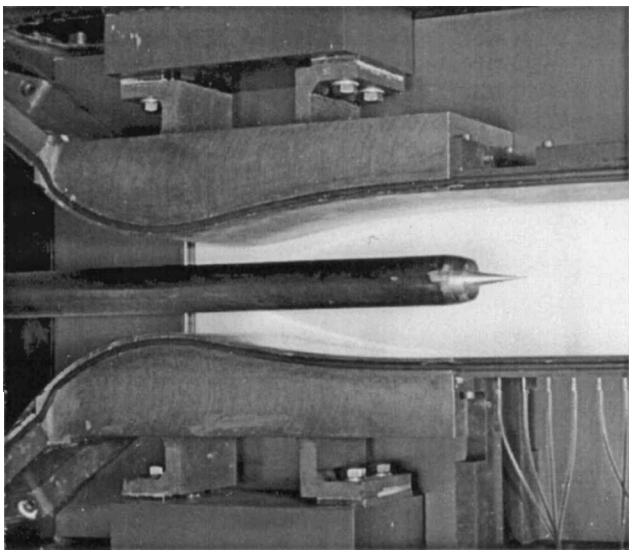

Fig. 11 Test setup with afterbody model in the S8Ch wind tunnel.

slot) control case with moderate mass flow rate ($Q = 0.016$ kg/s). A very intense suction of the boundary layer, localized at the slot origin, tends to strengthen the shock wave because the spreading caused by the interaction is reduced when compared with the reference case. Consequently, the entropy production through the shock system is more important and the efficiency loss higher. In addition, the thickening of the boundary layer is stabilized far downstream of the control region. This downstream stabilization leads to a reduction of the momentum loss compared to the reference case but not as large a reduction as that obtained in the distributed suction control case.

Flow Confluence and Afterbody Flow Interactions

Experimental Arrangement

The same tests were also conducted in the ONERA S8Ch research facility.[18,19] A photograph of the model setup in the test section of the continuous wind tunnel is shown in Fig. 11. The stagnation pressure p_{te} and the stagnation temperature T_{te} were approximately $(0.99 \pm 0.0005) \times 10^5$ Pa and 297 ± 5 K, respectively. The 120×120 mm test section was equipped with a two-dimensional nozzle designed to give a uniform Mach number close to 1.95. The axisymmetric afterbody model is mounted at the end of the 40-mm-diam central sting that is fixed upstream of the wind tunnel nozzle throat. The diameter of the model also equals 40 mm. The model consists of a central annular plug nozzle mounted inside a hollow cylinder. The cylinder is enclosed by a boattail and a small base. The contours of two full-length annular plug nozzles (noted as Mj2 and Mj3 nozzles) were calculated by the method of characteristics in order to provide, in the theoretical case of a perfectly adapted jet, a uniform flow with Mach numbers equal to 2 and 3, respectively, in the section at the end of the spike.[6] The plug nozzles were fed by dessicated room-temperature air. The jet stagnation pressure was varied from 1 to $10 \pm 0.05 \times 10^5$ Pa.

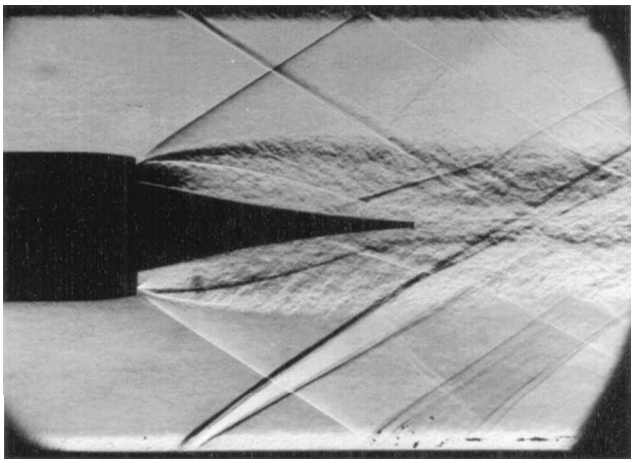

a) Mj3 nozzle (p_{tj}/p_{te} = 5.16)

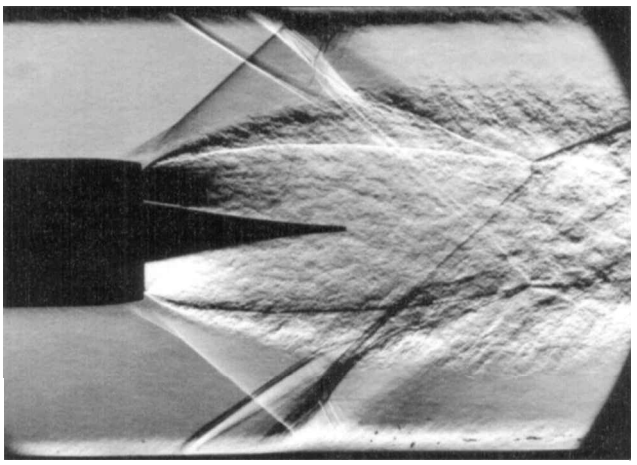

b) Mj2 nozzle (p_{tj}/p_{te} = 5.05)

Fig. 12 Spark schlieren photographs of the afterbody flowfields.

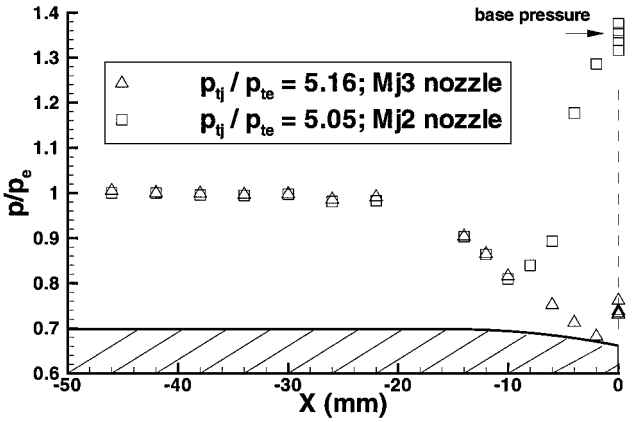

Fig. 13 Wall-pressure distributions on the boattail.

Flowfield Visualizations

Spark schlieren photographs were obtained with a Nanolite micropulser light source, allowing a 20-ns exposure time. The photographs, shown in Figs. 12a and 12b, give the main features of the afterbody flowfields obtained for the Mj3 and Mj2 nozzles at nearly the same pressure ratio (p_{tj}/p_{te} is approximately 5). For the Mj3 configuration, the jet-to-outer-flow stagnation pressure ratio is 5.16, which ratio corresponds to a reference static pressure ratio p_j/p_e equal to 1.1. The expansion fans centered at the nozzle lip confirm the underexpansion regime of the jet, which is associated by the forming of an internal shock or barrel shock. After flow separation, occurring near the end of the boattail for the external stream and near the nozzle lip for the jet, the flow boundaries envelop a small dead-air region downstream from the base. The mutual deflection of the flows due to flow confluence generates an external shock and the deflection of the internal shock. As a consequence, the barrel shock impinges on, then reflects from, the wall of the spike, which actions induce an interaction process with the developing boundary layer.

The Mj2 nozzle configuration (Fig. 12b), which has a higher static pressure ratio ($p_j/p_e = 5.05$), generates a stronger underexpansion of the jet. Since the underexpanded jet acts as a "fluid ramp" facing the incoming external flow, this jet pluming effect induces a shock-wave/boundary-layer interaction on the boattail and separation of the external boundary layer. The interaction shock coalesces with the confluence shock crossing the external flow. Once the two separated flows have merged downstream from the base, a wake develops and ensures the mutual adaptation of the flows. In this strongly underexpanded jet case, the nozzle flow is perturbed by expansion waves reflecting on the spike, while the barrel shock reflects far downstream of the plug nozzle. In fact, the reflected shock of the outer flow confluence is observed to interact with the barrel shock. This parasitic phenomenon prevents the barrel shock from reflecting on the symmetry axis.

Pressure Measurements

Wall-pressure measurements on the afterbody have been achieved using 28 0.4-mm-diam static pressure taps on the model. Figure 13 presents the wall-pressure distributions measured on the boattail, normalized by the upstream static pressure p_e for the Mj2 and Mj3 configurations. The two series of four pressure taps, each located on a circumference line around the boattail at the streamwise stations $X = -14$ and -26 mm, indicate good symmetry of the upstream flow. This symmetry is also confirmed with the four pressure taps on the base. On the cylindrical part of the model, the normalized static pressure is close to unity. As the flow expands when it reaches the boattail, the static pressure decreases.

For the Mj3 nozzle (Fig. 13), one cannot observe any pressure rise at the end of the boattail; however, we notice that the mean base pressure value, $p_B/p_e = 0.741$, is greater than the last pressure tap, $p/p_e = 0.672$, located 2 mm upstream from the base edge. This increase confirms the existence of an incipient interaction process, barely visible in Fig. 12a. For the Mj2 configuration, the pressure curve, shown in Fig. 13, clearly reveals the shock/external boundary layer interaction resulting from the jet pluming (expansion), as observed in Fig. 12b. Indeed, at a certain location, between $X = -6$ and -10 mm, the pressure rises rapidly when the boundary layer crosses the narrow compression wave system always located at the foot of the interaction shock. This rapid pressure rise is observed on the final part of the boattail, up to the last pressure tap located 2 mm before the base edge. Even if the pressure distribution does not show a "plateau" region, the slight difference between the base pressure and the pressure at the extremity of the boattail (less than 5%) makes the onset of an effective separation probable. It is clear that for this configuration, extended separations should result in higher pressure ratios.

LDV Measurements

The LDV system has been used in its two-component version. The external stream was seeded with sprayed olive oil by means of a movable tube placed in the wind-tunnel plenum chamber. The seeding of the jet was ensured by submicron-sized (0.5-μm-diam) silica oxide particles injected far upstream from the model nozzle throat. For each configuration, about 2300 measurement points were recorded. The streamwise mean component of the external velocity u_e, in the uniform Mach number region at the station $X/D = -0.1$, was measured as 512 m/s. Considering the stagnation temperature (297 K), the mean freestream Mach number was equal to 1.981. These values are slightly higher than the nozzle design Mach number because of the presence of the central sting. The resulting unit Reynolds number is equal to 12.24×10^6 m^{-1}. According to LDV measurements made in the freestream outer flow, at stations $X/D = -1$ and -0.5, the approach boundary-layer thickness (δ_0) is 7.1 ± 0.1 mm.

Figure 14 shows the mean velocity vector field for the Mj2 nozzle. One can clearly see the outer flow expansion and the initial

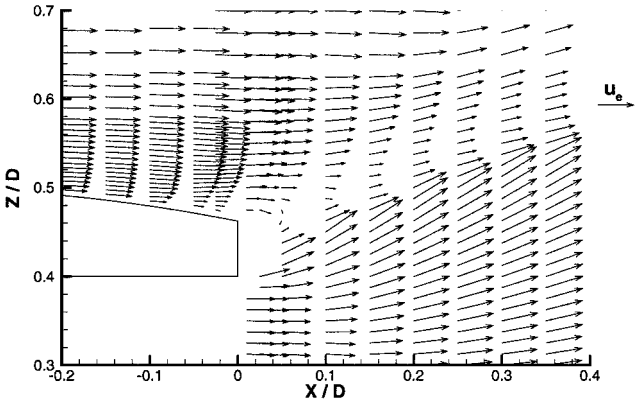

Fig. 14 Mean velocity vector field: magnified view of the base region (Mj2 nozzle).

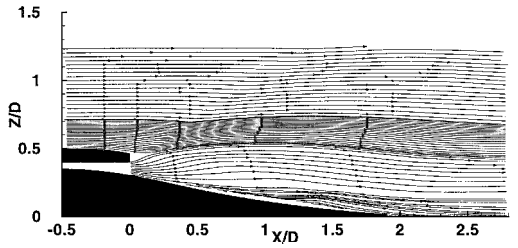

Fig. 15 Mean flow streamlines (Mj3 nozzle) ($p_{tj}/p_{te} = 4.99$).

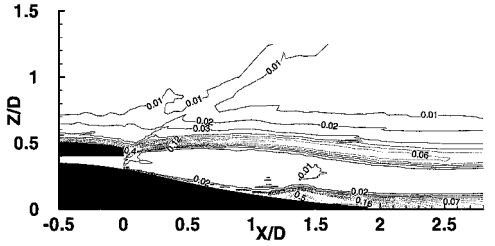

Fig. 16 Streamwise turbulence intensity (Mj3 nozzle) ($p_{tj}/p_{te} = 4.99$).

development of the mixing layers. No measurement point could be recorded very near the base surface because of the scarcity of seeding particles in this "dead-air" (recirculation) zone. The nearest station to the base that is completely measured is located at $X = 2$ mm, or $X/D = 0.05$. At this station, one can see that the streamwise component of the mean velocity becomes nearly equal to zero or can even be negative.

Figure 15 gives a magnified view of the mean flow streamlines in the spike region for the Mj3 nozzle.[20] The boundary layer that develops on the spike greatly thickens when the barrel shock impinges. However, when the laser beam approached the wall as close as possible, no separation or recirculation bubble was detected in the barrel shock reflection region. The LDV measurements allowed the determination of the components of the Reynolds tensor. The scalar field of the streamwise turbulence intensity σ_u, shown in Fig. 16, clearly reveals all the dissipative regions: the boundary layers developing on the boattail and on the spike, the separated shear layers, the wakes downstream from the confluence process and downstream from the spike, and the turbulence bubble in the reflection region of the barrel shock.

Conclusion

In the framework of the French PREPHA program, basic experiments have been carried out at the ONERA research facilities of the Chalais–Meudon Center. These tests allowed detailed experimental analyses that contributed to the improved understanding of the flow interactions that take place upstream, in scramjet air inlets, and around the afterbody of hypersonic spacecraft. These experimental data also provide test cases for the validation of design tools that will optimize the aerodynamic design of such propulsion systems.

The shock/shock interactions occurring upstream of the air inlet lip were simulated for laminar conditions by means of a shock generator and a cylinder located perpendicular to the freestream. First, the configuration with the cylinder alone was tested to provide comparisons between computations and experiments that have confirmed the validity of the DLCARS measurement technique. Then, measurements performed on configurations with the shock generator revealed the pressure and heat-flux peaks induced by type III and type IV shock interactions.

The shock-wave/boundary-layer interaction and its control were investigated in order to improve the performance of air inlets for future high-speed vehicles. The tested control devices employed active control by distributed suction through a perforated plate and by localized suction through a slot. The distributed suction control reduced the efficiency loss of the air inlet and limited the momentum loss, even with a moderate suction mass flow rate. This momentum loss could be reduced by optimizing the characteristics of the perforated plate, particularly its effective roughness. Localized suction control (by means of the slot) did not provide as beneficial an effect for the same moderate mass flow rate. The location of the slot relative to the impingement of the incident shock wave would be an interesting parameter to study in order to improve the efficiency of these active control devices.

The flow confluence between an external supersonic flow and the propulsive jet exhausting from a full-length annular aerospike nozzle was studied in underexpansion regimes. Two shock-wave/boundary-layer interactions occurring in such a propulsive afterbody were measured in detail. First, an interaction occurring on the boattail with incipient flow separation induced by the jet pluming (expansion). Second, an interaction with the boundary layer developing on the spike, which is caused by the reflection process of the jet barrel shock on the spike wall. The design of such external ramp nozzles must take into account the forming of interactions that could lead to severe negative consequences for the vehicle performance.

Acknowledgments

The present study has been performed under contract from the Délégation Générale pour l'Armement of the French Ministry of Defense. The authors would like to thank T. Pot, M. Lefebvre, and P. Bouchardy for the experiments performed with the DLCARS technique in the R5Ch wind tunnel; C. Marmignon for using the Homard2 code; B. Corbel and P. Molton for the experiments performed in the S8Ch wind tunnel; and R. Soares and D. Soulevant for performing the LDV measurements.

References

[1]Edney, B., "Anomalous Heat Transfer and Pressure Distributions on Blunt Bodies at Hypersonic Speeds in the Presence of an Impinging Shock," Aeronautical Research Inst. of Sweden, Rept. 115, Stockholm, 1968.

[2]Borovoy, V. Y., Chinilov, A. Y., Gusev, V. N., Struminskaya, I. V., Délery, J., and Chanetz, B., "Interference Between a Cylindrical Bow Shock and a Plane Oblique Shock," *AIAA Journal*, Vol. 35, No. 11, 1997, pp. 1721–1728.

[3]Mohamed, A. K., Pot, T., and Chanetz, B., "Diagnostics by Electron Beam Fluorescence in Hypersonics," *16th International Congress on Instrumentation in Aerospace Simulation Facilities*, IEEE Publications, Piscataway, NJ, 1995, pp. 14.1–14.4; also ONERA, Rept. TP-1995-84, 1995.

[4]Délery, J., "Shock-Wave/Turbulent Boundary-Layer Interaction and Its Control," edited by A. D. Young, *Progress in Aerospace Science*, Vol. 22, No. 4, 1985, pp. 209–280; also ONERA, Rept. TP-1984-27, 1984.

[5]Bur, R., "Control Devices Applied to Shock-Wave/Boundary-Layer Interactions: The PREPHA Program" ("Techniques de Contrôle des Interactions onde de Choc/Couche Limite. Programme PREPHA"), ONERA, Rept. RTS-97/7078AY, Châtillon, France, June 1993.

[6]Reijasse, P., and Délery, J., "Flow Confluence Past an Afterbody: General Overview and Description of the Experimental Set-Up," ONERA, Rept. RT-33/4361AY-AN, Châtillon, France, Dec. 1995.

[7]Chanetz, B., and Coët, M.-C., "Shock-Wave/Boundary-Layer Interaction Analyzed in the R5Ch Wind Tunnel," *Aerospace Research*, No. 1993-5, 1993, pp. 43–56.

[8]Pot, T., Chanetz, B., Lefebvre, M., and Bouchardy, P., "Fundamental Study of Shock/Shock Interferences in Low-Density Flow: Flowfield Measurements by DLCARS," *Proceedings of the 21st Rarefied Gas Dynamics Symposium*, edited by R. Brun, R. Campargue, R. Gatignol, and

J.-C. Lengrand, Cepadues Editions, Vol. 2, Marseille, France, 1999; also ONERA, Rept. TP-1998-140, 1998.

[9]Lefebvre, M., Chanetz, B., Pot, T., Bouchardy, P., and Varghese, P., "Measurement by Coherent Anti-Stokes Raman Scattering in the R5Ch Hypersonic Wind Tunnel," *Aerospace Research*, No. 1994-4, 1994, pp. 295–298.

[10]Hollanders, H., and Marmignon, C., "Navier–Stokes High Speed Flow Calculations by an Implicit Non-Centered Method," AIAA Paper 89-0282, Jan. 1989.

[11]Berry, S. A., and Nowak, R. J., "Fin Leading-Edge Sweep Effect on Shock/Shock Interaction at Mach 6," *Journal of Spacecraft and Rockets*, Vol. 34, No. 4, 1997, pp. 416–425.

[12]Moss, J. N., Pot, T., Chanetz, B., and Lefebvre, M., "DSMC Simulation on Shock/Shock Interactions: Emphasis on Type IV Interactions," *22nd International Symposium on Shock Waves*, London, Paper 3570, July 1999; also ONERA, Rept. TP-1999-107, 1999.

[13]Bur, R., and Molton, P., "Experimental Studies on Shock-Wave/Boundary-Layer Interaction Control. The PREPHA Program" ("Etudes Expérimentales sur le Contrôle des Interactions onde de Choc/Couche Limite. Programme PREPHA"), ONERA, Rept. RTS-108/7078AY, Châtillon, France, April 1996.

[14]Boutier, A., d'Humières, C., and Soulevant, D., "Three-Dimensional Laser Velocimetry: A Review," *2nd International Symposium on Applications of Laser Anemometry to Fluid Mechanics*, edited by D. F. G. Durão, Lisbon, 1984, pp. 1–10.

[15]Délery, J., and Marvin, J. G., "Shock-Wave/Boundary-Layer Interactions," AGARDograph 280, edited by E. Reshotko, 1986, pp. 3–108.

[16]Bur, R., Délery, J., and Corbel, B., "Basic Study of Passive Control Applied to a Two-Dimensional Transonic Interaction," *Notes on Numerical Fluid Mechanics*, edited by E. Stanewsky, J. Délery, J. Fulker, and W. Geissler, Vol. 56, Vieweg, Brunswick, Germany, 1997, pp. 89–111.

[17]Bur, R., Corbel, B., and Délery, J., "Study of Passive Control in a Transonic Shock-Wave/Boundary-Layer Interaction," *AIAA Journal*, Vol. 36, No. 3, 1998, pp. 394–400.

[18]Reijasse, P., and Corbel, B., "Basic Experiments on Non-Adaptation Phenomena in Aerospike Nozzles," AIAA Paper 97-2303, June 1997.

[19]Reijasse, P., Corbel, B., and Délery, J., "Flow Confluence Past a Jet-On Axisymmetric Afterbody," *Journal of Spacecraft and Rockets*, Vol. 34, No. 5, 1997, pp. 593–601.

[20]Coponet, D., Corbel, B., Délery, J., de La Forest Divonne, C., and Reijasse, P., "Experimental Analysis of Supersonic Flow Confluence Downstream Axisymmetric Afterbodies. The PREPHA Program" ("Analyse Expérimentale de la Confluence d'Écoulements Supersoniques en Aval d'Arrière-Corps de Révolution. Deuxième Série d'Essais. Programme PREPHA"), ONERA, Rept. RT-43/4361 DAFE/AY, Châtillon, France, Nov. 1998.

M. Torres
Associate Editor

Color reproductions courtesy of the French Ministry of Defense.